Nonreciprocal magnons in a two-dimensional crystal with out-of-plane magnetization

Marcio Costa,[1] N. M. R. Peres,[2,3] J. Fernández-Rossier,[2,*] and A. T. Costa [2]

[1]*Instituto de Física, Universidade Federal Fluminense, 24210-346 Niterói, RJ, Brazil*
[2]*QuantaLab, International Iberian Nanotechnology Laboratory, 4715-330 Braga, Portugal*
[3]*Centro de Física das Universidades do Minho e Porto and Departamento de Física and QuantaLab, Universidade do Minho,
Campus de Gualtar, 4710-057 Braga, Portugal*

Nonreciprocal spin waves have a chiral asymmetry so that their energy is different for two opposite wave vectors. They are found in atomically thin ferromagnetic overlayers with in-plane magnetization and are linked to the antisymmetric Dzyaloshinskii-Moriya surface exchange. We use an itinerant fermion theory based on first-principles calculations to predict that nonreciprocal magnons can occur in Fe_3GeTe_2, the first stand-alone metallic two-dimensional crystal with out-of-plane magnetization. We find that both the energy and lifetime of magnons are nonreciprocal, and we predict that acoustic magnons can have lifetimes up to hundreds of picoseconds, orders of magnitude larger than in other conducting magnets.

I. INTRODUCTION

A defining property of elementary excitations in crystals such as electrons, excitons, phonons, plasmons, and magnons is their dispersion curve $E(\vec{q})$. In most cases, the dispersion curves satisfy the reciprocity relation $E(\vec{q}) = E(-\vec{q})$, reflecting the equivalence between the excitation and its mirror image, i.e., their nonchiral nature. In condensed-matter systems, nonreciprocal energy dispersions occur under specific circumstances and elicit great attention. Examples are chiral [1] and helical [2] edge states of topological phases of various excitations, including electrons, photons, and magnons, as well as Rashba split bands in crystals lacking inversion symmetry and having strong spin-orbit coupling [3].

A major driving force for chiral phenomena in magnetism [4–6] is the antisymmetric exchange $\vec{D}_{ij} \cdot (\vec{S}_i \times \vec{S}_j)$, proposed by Dzyaloshinskii [7] and Moriya [8] (DM). This special type of superexchange is enabled by the combination of spin-orbit coupling [8] and the absence of an inversion center between spins i, j. These conditions are naturally found in overlayers of atomically thin ferromagnets on top of surfaces with high spin-orbit coupling. With this background, the existence of nonreciprocal spin waves was predicted [9,10], provided that the DM vector $\vec{D}$ is parallel to the magnetization $\vec{M}$. Symmetry considerations for this class of systems [11] leads to the conclusion that the interfacial $\vec{D}$ lies in plane so that nonreciprocal spin waves in interfaces can only exist for ferromagnets with in-plane easy axis, consistent with experimental observations [12,13]. Logical devices based on nonreciprocal spin waves have been recently proposed [14]. Chirality-dependent Stoner damping has also been predicted for half-metallic ferrimagnets [15].

In this work we show that nonreciprocal spin waves can exist in a newly discovered class of two-dimensional (2D) magnets [16], stand-alone 2D crystals with out-of-plane magnetization. The survival of magnetism in 2D is definitely linked to a strong spin-orbit coupling that opens up a gap in the magnon spectrum, preventing the infrared catastrophe that destroys long-range order in isotropic 2D magnets, as shown by Mermin and Wagner [17], inspired [18] by Hohenberg [19].

Here we explore magnons of Fe_3GeTe_2 for several reasons. First, it has a low-symmetry magnetic unit cell without an inversion center. Second, the observation of large anomalous Hall effect [20], anomalous Nernst effect [21], and skyrmions [22] in thin films strongly suggests that intrinsic DM interaction, as opposed to interfacial, is active in Fe_3GeTe_2. Third, the system is a conductor, unlike other widely studied 2D crystals such as CrI_3, and has a large Curie temperature that can reach room temperature upon gating [23]. Fe_3GeTe_2 was synthesized for the first time in bulk in 2006 [24]. Much more recently, however, high-quality few-layer samples have been produced [25]. Monolayers have been obtained by exfoliation [26].

Because of its conducting nature and high-temperature ordering, Fe_3GeTe_2 is closer to technological applications. On the theory side, modeling magnons in conducting ferromagnets represents a big challenge due to the noninteger nature of the magnetic moments, the long-range exchange, and the damping of magnons due to their coupling to Stoner excitations [27–33]. A microscopic description that does not take the itinerant character into account, such as that provided by spin models, will fail to describe most of the relevant physics of these systems. Spin models can, however, provide valuable insight about the nature of spin fluctuations in itinerant ferromagnets, as long as the appropriate care is exercised in building the model, drawing conclusions, and formulating physical interpretations. At low excitation energies, for which the density of Stoner modes tends to be small, the results

---

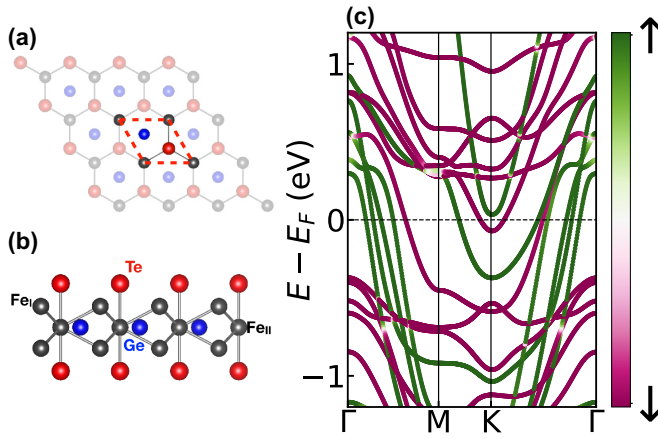*On leave from Departamento de Física Aplicada, Universidad de Alicante, 03690 San Vicente del Raspeig, Spain.

FIG. 1. Top (a) and side (b) views of the lattice structure showing the unit cell [marked by the dashed red line in (a) and the two nonequivalent Fe sites in (b)]. In (c) we show the band structure along high-symmetry points in the 2D Brillouin zone [depicted in the inset of Fig. 3(a)]. The color code shows the projection of the electronic eigenvectors on the eigenstates of S_z.

derived from itinerant and localized descriptions usually agree well. The issue of choosing which terms to include in the localized spin description, however, frequently poses a hard problem, especially in systems with long-range interactions and low symmetry. This will become clear as we present and discuss our results.

The paper is organized as follows: in the next section we present the theoretical methods we employed, in Sec. III we present and discuss our results, and in Sec. IV we offer a summary and some concluding remarks.

II. METHODS

We compute the magnon spectra of a Fe_3GeTe_2 monolayer using the itinerant fermion picture [10,34]. With this method we are able to extract magnon energies and lifetimes from a first-principles electronic structure calculation, without the need of building an intervening effective spin model. We use density functional theory (DFT) [35,36] to derive an effective fermionic Hamiltonian to describe the spin dynamics of 2D materials. The unit cell of Fe_3GeTe_2 is shown in Fig. 1. It has three Fe atoms occupying two nonequivalent positions, A and B. We denote them Fe^A, Fe^{B_1}, and Fe^{B_2}. There is no inversion center along the lines joining Fe^A and $Fe^{B_{1,2}}$.

The DFT calculations were performed using the plane-waves code QUANTUM ESPRESSO [37]. The electronic exchange correlation is described by the generalized gradient approximation (GGA) within the Perdew-Burke-Ernzerhof (PBE) functional [38]. Ionic cores are described using projector augmented wave (PAW) pseudopotentials [39]. The local effective paramagnetic Hamiltonian is obtained using a direct projection of the Kohn-Sham states onto a pseudoatomic orbital (PAO) basis [40] as implemented in the PAOFLOW code [41].

The PAO tight-binding Hamiltonian is constructed using a *spd* basis for Fe, Ge, and Te atoms. We then add local spin-orbit coupling and intra-atomic Coulomb repulsion [42]. The spin-orbit coupling strengths of Fe, Ge, and Te are

$\lambda_{Fe} = 50$ meV, $\lambda_{Ge} = 200$ meV, $\lambda_{Te} = 600$ meV [43]. Electronic bands calculated using these values reproduce with high-accuracy spin-orbit-coupling–induced gaps at high-symmetry points in the Brillouin zone calculated using DFT. The mean-field self-consistent ground state is obtained [34,44] by treating every component of the spin moment in each Fe atom as an independent variable. The resulting band structure, shown in Fig. 1, features several spin-polarized bands at the Fermi energy, portraying Fe_3GeTe_2 as a ferromagnetic conductor.

We find that the mean-field spin moments are $s_{B_1} = s_{B_2} = 2.56\mu_B$ and $s_A = 1.52\mu_B$, all of them along the out-of-plane axis. These values are in excellent agreement with the DFT results, $s_{B_1} = s_{B_2} = 2.54\mu_B$ and $s_A = 1.52\mu_B$. The spin moments of Te and Ge are negligible. We note that given that the magnetic moments are approximately twice the spin values, the tentative spin values of Fe atoms are clearly not quantized as half-integers, which is a distinguishing feature of itinerant ferromagnets.

The key quantity in the itinerant fermion theory for spin excitations [10,34] is the spin-flip spectral density $\mathcal{S}(E, \vec{q}) \equiv Im[\chi^\perp(E, \vec{q})]$, where

$$\chi_{ll'}^\perp(E, \vec{q}) \equiv \int_{-\infty}^\infty dt e^{-i\frac{E}{\hbar}t}\{-i\theta(t)\langle[S_{l,\vec{q}}^+(t), S_{l',-\vec{q}}^-(0)]\rangle\}, \quad (1)$$

l, l' label the atomic site within the unit cell, E is the excitation energy, $\vec{q}$ is the magnon wave vector, $\theta(t)$ is the Heaviside unit step function,

$$S_{l,\vec{q}}^+ \equiv \sum_{\vec{k}} a_{l,\vec{k}\uparrow}^\dagger a_{l,\vec{k}+\vec{q}\downarrow}, \quad (2)$$

$$S_{l,\vec{q}}^- \equiv \sum_{\vec{k}} a_{l,\vec{k}\downarrow}^\dagger a_{l,\vec{k}+\vec{q}\uparrow}, \quad (3)$$

where $a_{l,\vec{k}\sigma}^\dagger$ is a creation operator for electrons, and $\langle\cdot\rangle$ denotes thermal average. The four-fermion correlator in Eq. (1) is computed in the random phase approximation (RPA) [10,29,34]. In the absence of spin-orbit coupling, the spin-flip, or transverse, spin susceptibility completely determines the behavior of the magnons, since transverse fluctuations of the spin density are decoupled from longitudinal spin fluctuations and from charge fluctuations. However, when SOC is taken into account, all those fluctuations are coupled. Within the RPA this entails a set of coupled linear equations that determine simultaneously the spin-flip susceptibility and three other propagators,

$$\chi_{ll'}^{3-}(t, \vec{q}) \equiv -i\theta(t)\langle[S_{l,\vec{q}}^z(t), S_{l',-\vec{q}}^-(0)]\rangle,$$
$$\chi_{ll'}^{q-}(t, \vec{q}) \equiv -i\theta(t)\langle[n_{l,\vec{q}}(t), S_{l',-\vec{q}}^-(0)]\rangle, \quad (4)$$
$$\chi_{ll'}^{--}(t, \vec{q}) \equiv -i\theta(t)\langle[S_{l,\vec{q}}^-(t), S_{l',-\vec{q}}^-(0)]\rangle,$$

where

$$n_{l,\vec{q}} \equiv \sum_{\vec{k}}(a_{l,\vec{k}\uparrow}^\dagger a_{l,\vec{k}+\vec{q}\uparrow} + a_{l,\vec{k}\downarrow}^\dagger a_{l,\vec{k}+q\downarrow}). \quad (5)$$

As we will show momentarily, the strength of the coupling between transverse spin fluctuations and longitudinal and charge fluctuations in Fe_3GeTe_2 is small enough so that we can restrict our analysis to the spin-flip spectral density.
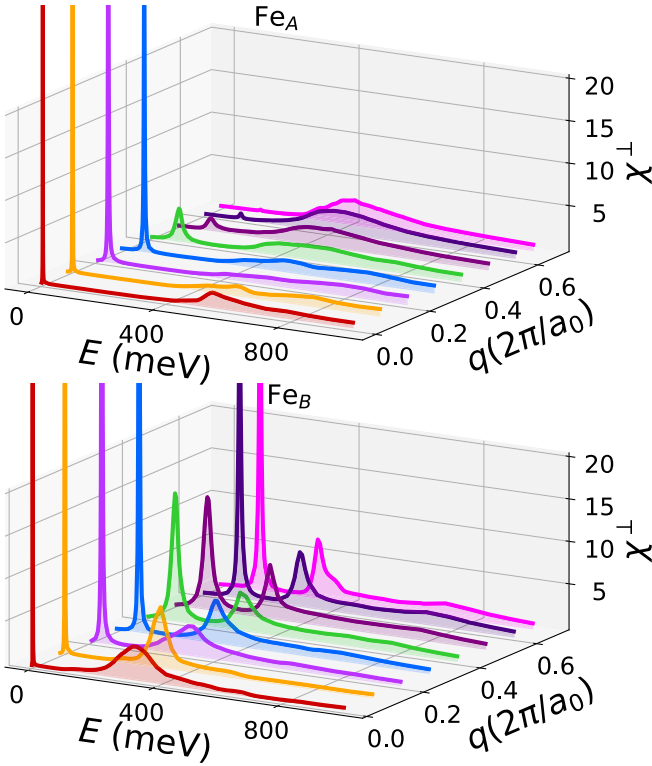
FIG. 2. Magnon spectral density projected at the two nonequivalent Fe sites as a function of energy for a few selected wave vectors along the $\Gamma - K$ direction. The sharp peak at low energies is associated with the "acoustic" magnon, and the broad structure at energies $\sim$300 meV is the (strongly damped) "nonbonding" magnon.

III. RESULTS AND DISCUSSION

The diagonal entries, $\chi_{AA}^{\perp}(E, \vec{q})$ and $\chi_{B_1B_1}^{\perp}(E, \vec{q}) = \chi_{B2B2}^{\perp}(E, \vec{q})$, of the spin-flip spectral density are shown in Fig. 2 for a few selected wave vectors. For a given value of $\vec{q}$ the spin-flip spectral density has, in general, two types of features. First, there are symmetric peaks, with a width ΔE much smaller than peak energy E. These peaks are not present in the spectral density of the noninteracting susceptibility. These are magnons modes, featured by all ferromagnets. Second, there are broad asymmetric features that correspond to the so-called Stoner excitations and are only present in conducting ferromagnets.

To assess the relative importance of the coupling between transverse spin fluctuations and their charge and longitudinal spin counterparts, we compared the peak values of $\chi_{ll'}^{3-}$ and $\chi_{ll'}^{q-}$, defined in Eq. (4), with the peak value of the spin-flip spectral density at the same wave vector. The largest value of $|\chi_{ll'}^{3-}|$ for all wave vectors we considered are never more than 2% of the spin-flip spectral weight. $|\chi_{ll'}^{q-}|$ is at least one order of magnitude smaller than $|\chi_{ll'}^{3-}|$ for all wave vectors considered. Thus, we can safely assume the contribution of non-spin-flip fluctuations to the excited states of the system is negligible when compared to transverse fluctuations.

Two well-defined magnon branches are identified in Fig. 2. For reasons that will become apparent later, we refer to the lower energy, narrow peaks as the acoustic branch and to the
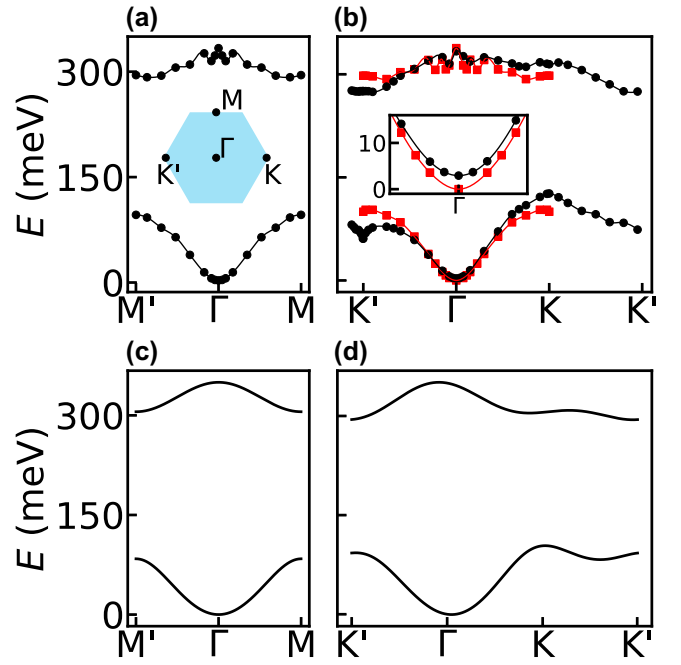

FIG. 3. Fe_3GeTe_2 magnon dispersion relation along high-symmetry lines in the 2D Brillouin zone. The dispersion relation along Γ-M (a) is reciprocal, whereas along $\Gamma - K$ (b, black circles) it shows strong nonreciprocity. In the inset we show a zoom of the dispersion relation for the acoustic magnon close to the Γ point, where the magnetocrystalline anisotropy gap $\Delta_{\Gamma} \equiv E(\Gamma) = 2.93$ meV can be clearly seen. For comparison, we also show the dispersion relation calculated without spin-orbit coupling (red squares), which is perfectly reciprocal and shows no anisotropy gap, as expected. In (c) and (d) we show the dispersion relations obtained with the localized spin model, including the second-neighbor Dzyaloshinskii-Moriya coupling. The Brillouin zone is shown in the inset of panel (a).

higher energy, broader peaks as the nonbonding branch. When SOC is included, the acoustic branch has a gap at the Γ point $\Delta_{\Gamma} = 2.9$ meV that accounts for the magnetic anisotropy. Its magnitude is compatible with existing measurements [45] and DFT calculations [46]. The acoustic branch has weight distributed between A and B sublattices, although most of it lies on the B sites. In contrast, the nonbonding branch is missing entirely from the A site. A broad feature appears at higher ($\gtrsim$400 meV) energies, localized in the A site, whose nature is discussed below.

The magnon dispersion relation along high-symmetry lines in the Brillouin zone is shown in Fig. 3, calculated both with and without spin-orbit coupling. The bandwidth of the acoustic magnon ($\sim$120 meV) is much larger than that obtained in other 2D magnets, such as CrI_3 [34], and reflects a large exchange coupling between the magnetic moments in neighboring Fe atoms, in line with the larger Curie temperature of Fe_3GeTe_2.

Importantly, when the SOC is included in the calculation, both the acoustic and the nonbonding bands become nonreciprocal in the $K - \Gamma - K'$ direction but not on the $\Gamma - M$ direction. It is noteworthy that the dispersion relation of the acoustic mode around the Γ point fits almost perfectly to a function of wave vector $\vec{q}$ of the form $\Delta_{\Gamma} + Dq^2$, with

a negligible linear component. This is in contrast with the behavior of magnons in ultrathin transition-metal films on heavy substrates [10], where a sizable linear term is induced by the DM coupling, and has also been observed in relation to the calculation of static spin spirals in Fe_3GeTe_2 [47].

At this point we introduce a model Hamiltonian for the magnons in order to gain physical insight into the origin of the most salient features of the results obtained with the itinerant model. The departure point is a spin Hamiltonian

$$\mathcal{H} = \mathcal{H}_{\text{Heis}} + \mathcal{H}_{\text{DM}} + \mathcal{H}_{\text{anis}}, \tag{6}$$

composed of an isotropic Heisenberg term $\mathcal{H}_{\text{Heis}}$, a Dzyaloshinskii-Moriya interaction $\mathcal{H}_{\text{DM}}$, and a single-ion anisotropy term $\mathcal{H}_{\text{anis}}$. Explicit expressions and further detail can be found in the Supplemental Material (SM) [48]. We build the magnon model using the conventional Holstein-Primakoff linear spin-wave theory for a quantized spin model.

The spins live in a *decorated honeycomb* lattice with three sites per unit cell, A, B_1, B_2 (see Fig. 1 of the SM [48]), with spins S_A and S_B. Given that sites B_1 and B_2 are equivalent, we can introduce two modes, symmetric and antisymmetric combinations of B_1 and B_2, so that one of them becomes effectively decoupled from A. The decoupling naturally leads to three bands. One is associated with the antisymmetric B mode. The other two describe a honeycomb ferromagnet with broken inversion symmetry on account of the different nature of A and B, and are separated by a gap. The projections of the magnon wave functions over the different sites (see Fig. 3 in the SM [48]) show that the spin model naturally accounts for the fact that the acoustic branch is predominantly located in the symmetric B mode, the $\vec{k}$ dependence of the weight on the A site, and the complete localization of the nondispersive band on the B mode. This behavior is qualitatively identical to that of the magnon wave functions extracted directly from the fermionic model (see SM [48] for details).

We are now in a position to address the origin of the nonreciprocal dispersion, obtained with the itinerant model, using the spin model. The fact that it only arises when spin-orbit coupling is included is a clear indication that the origin has to come from the non-Heisenberg terms in the Hamiltonian. We have considered both first- and second-neighbor DM couplings, $D^{(1)}_{a,a'}$ and $D^{(2)}_{a,a'}$, where a, a' label the sites in the unit cell that do not possess an inversion center. We only consider the DM vector $\vec{D}$ parallel to the magnetization, i.e., in the out-of-plane direction.

We find that first- and second-neighbor DM coupling yield nonreciprocal dispersions. However, only a finite $D^{(2)}$ coupling for the B sublattice gives a nonreciprocal dispersion in the $K - \Gamma - K'$ line and reciprocal dispersion along the $\Gamma - M$ direction. Therefore the nonreciprocal dispersion is consistent with a second-neighbor DM interaction in the B sublattice for which the superexchange pathways occur via tellurium atoms, the ones with the largest SOC in the crystal. It is worth mentioning that this term also introduces a linear contribution to the dispersion relation around the Γ point. This is in disagreement with the results from the itinerant fermion model. The most probable reason for this discrepancy is the existence of more DM coupling terms arising through diverse superexchange pathways, which compensate the lin-
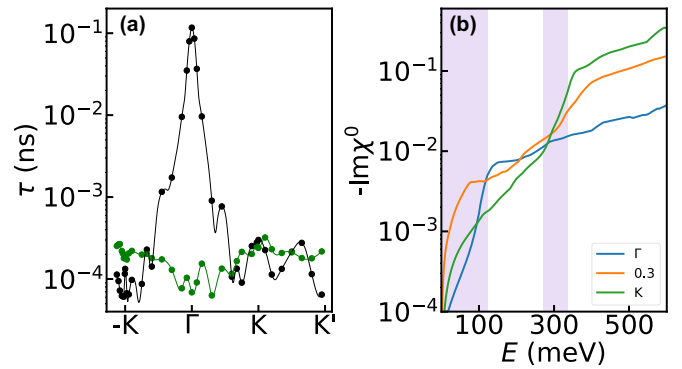

FIG. 4. (a) Magnon lifetimes as a function of wave vector for the acoustic (black circles) and nonbonding (green circles) branches. (b) Spectral density of Stoner modes as a function of energy for three different wave vectors along the $\Gamma - K$ line. The shaded regions mark the bandwidths of the acoustic and nonbonding magnons.

ear term arising from $D^{(2)}$ alone. This issue will be further explored elsewhere.

We now shift our attention to one of the hallmarks of itinerant magnetism: the fact that magnons have finite lifetimes because of their coupling with the continuum of uncorrelated electron-hole excitations known as the Stoner continuum. In Fig. 4(a) we show the magnon lifetimes as a function of wave vector. The lifetime is related to the linewidth of the spectral density via $\tau \equiv \frac{2\hbar}{\Delta E}$. Remarkably, the acoustic magnons close to the Γ point have very long lifetimes ($\sim$100 ps), given that the longest lifetimes measured in ultrathin conducting magnets [49] are $\sim$0.4 ps. A long magnon lifetime is a very important figure of merit for potential applications of magnons as carriers of information, for example.

The lifetime of a magnon with energy E and wave vector $\vec{q}$ scales inversely with the weight of the Stoner spectral density at the same energy and wave vector. Due to the spin polarization of the d bands, the density of Stoner modes is very small for energies much smaller than the exchange splitting, which is roughly proportional to magnetization and the intra-atomic Coulomb repulsion strength. For Fe_3GeTe_2 the exchange splitting is $\sim$1.5 eV. The Stoner spectral density grows abruptly as the excitation energy becomes of the order of the exchange splitting, as seen in Fig. 4(b). For Fe_3GeTe_2, the energies of acoustic magnons lie in the region of small density of Stoner modes, whereas the nonbonding magnons live in the energy range where the Stoner spectral density is considerable. This is the origin of the large difference between acoustic and nonbonding magnon lifetimes.

In this context we can understand why the itinerant picture leads to only two magnon modes, whereas the localized spin model has three. Basically, the third magnon band, still higher in energy than the second, is degenerate with the continuum of Stoner spin-flip excitations. As a result, the spectral weight of the high-energy optical magnon mode is transferred to the incoherent features, predominantly localized in the A site, shown in Fig. 2. The difference between the two theories highlights the limitations of the spin Hamiltonian, most notably in the case of itinerant magnets. The overdamping of high-energy magnons by the Stoner continuum has been

extensively explored in the context of ultrathin ferromagnetic films on metallic substrates [27–29,32,33]. In that class of systems the hybridization between the spin-polarized electronic states of the ferromagnetic film with the spin-unpolarized states of the metallic substrate introduces a high density of Stoner modes at relatively low energies.

The acoustic magnon lifetimes are also nonreciprocal. This effect is *not* exclusively related to the nonreciprocity of the energy dispersion: lifetimes are shorter in general for higher energy states. We find that although magnons around the K point have both energies and lifetimes larger than those at K', the ultimate reason for the nonreciprocal lifetimes stems from the fact that the density of Stoner modes in Fe_3GeTe_2 is also nonreciprocal.

Besides endowing magnons with finite lifetimes, the Stoner continuum renormalizes the magnon energies, much like friction changes the natural frequency of a harmonic oscillator. This is the origin of the oscillations in the dispersion relation of the nonbonding magnons, seen in Fig. 3(b). The dispersion relation of the acoustic magnons close to the K point also displays some oscillations of the same origin.

IV. CONCLUDING REMARKS

In conclusion, we have calculated magnons in monolayer Fe_3GeTe_2 using an itinerant fermion description derived from first-principles calculations, and we have compared those results with the simple magnon theory for a spin model Hamiltonian for a decorated honeycomb lattice with three spins per unit cell. Due to broken mirror symmetry and spin-orbit coupling, magnon energies and lifetimes show nonreciprocal behavior along the $\Gamma - K$ direction. Our findings are consistent with a second-neighbor DM coupling in the B sublattice, but this deserves further attention. The coupling of magnons to Stoner excitations results in an intrinsic broadening of the two lowest energy magnon branches and the melting of the optical mode, expected in the spin model, into a broad spectral feature at high energies. From our results, we infer a value for the spin-wave stiffness A that is compatible with the large magnetic transition temperatures observed experimentally, namely, $A \approx 513$ meV Å^2. For comparison, the spin-wave stiffness constant for yttrium iron garnet, a widely used ferromagnetic insulator, has been recently inferred from neutron scattering measurements to be 532 meV Å^2 [50]. Furthermore, we find that the acoustic magnons are extremely long lived for a conducting two-dimensional ferromagnet ($\tau \sim 100$ ps at the Γ point), which makes this material potentially very useful for magnonics and spintronics applications. Our work shows that nonreciprocal magnons can exist in 2D crystals with out-of-plane magnetization due to their intrinsic DM interaction and suggest that Fe_3GeTe_2 is a very interesting material to explore nontrivial magnon effects.

[1] F. D. M. Haldane, Phys. Rev. Lett. **61**, 2015 (1988).

[2] C. L. Kane and E. J. Mele, Phys. Rev. Lett. **95**, 226801 (2005).

[3] D. Xiao, G.-B. Liu, W. Feng, X. Xu, and W. Yao, Phys. Rev. Lett. **108**, 196802 (2012).

[4] M. Hervé, B. Dupé, R. Lopes, M. Böttcher, M. D. Martins, T. Balashov, L. Gerhard, J. Sinova, and W. Wulfhekel, Nat. Commun. **9**, 1015 (2018).

[5] M.-G. Han, J. A. Garlow, Y. Liu, H. Zhang, J. Li, D. DiMarzio, M. W. Knight, C. Petrovic, D. Jariwala, and Y. Zhu, Nano Lett. **19**, 7859 (2019).

[6] B. Ding, Z. Li, G. Xu, H. Li, Z. Hou, E. Liu, X. Xi, F. Xu, Y. Yao, and W. Wang, Nano Lett. **20**, 868 (2020).

[7] I. E. Dzyaloshinskii, Sov. Phys. JETP **5**, 1259 (1957).

[8] T. Moriya, Phys. Rev. **120**, 91 (1960).

[9] L. Udvardi and L. Szunyogh, Phys. Rev. Lett. **102**, 207204 (2009).

[10] A. T. Costa, R. B. Muniz, S. Lounis, A. B. Klautau, and D. L. Mills, Phys. Rev. B **82**, 014428 (2010).

[11] A. Crépieux and C. Lacroix, J. Magn. Magn. Mater. **182**, 341 (1998).

[12] K. Zakeri, Y. Zhang, J. Prokop, T.-H. Chuang, N. Sakr, W. X. Tang, and J. Kirschner, Phys. Rev. Lett. **104**, 137203 (2010).

[13] K. Zakeri, Y. Zhang, T.-H. Chuang, and J. Kirschner, Phys. Rev. Lett. **108**, 197205 (2012).

[14] M. Jamali, J. H. Kwon, S.-M. Seo, K.-J. Lee, and H. Yang, Sci. Rep. **3**, 3160 (2013).

[15] M. M. Odashima, A. Marmodoro, P. Buczek, A. Ernst, and L. Sandratskii, Phys. Rev. B **87**, 174420 (2013).

[16] C. Gong and X. Zhang, Science **363**, eaav4450 (2019).

[17] N. D. Mermin and H. Wagner, Phys. Rev. Lett. **17**, 1133 (1966).

[18] B. I. Halperin, J. Stat. Phys. **175**, 521 (2019).

[19] P. C. Hohenberg, Phys. Rev. **158**, 383 (1967).

[20] K. Kim, J. Seo, E. Lee, K.-T. Ko, B. S. Kim, B. G. Jang, J. M. Ok, J. Lee, Y. J. Jo, W. Kang, J. H. Shim, C. Kim, H. W. Yeom, B. Il Min, B.-J. Yang, and J. S. Kim, Nat. Mater. **17**, 794 (2018).

[21] J. Xu, W. A. Phelan, and C.-L. Chien, Nano Letters **19**, 8250 (2019).

[22] T.-E. Park, L. Peng, J. Liang, A. Hallal, X. Zhang, S. Jong Kim, K. M. Song, K. Kim, M. Weigand, G. Schuetz, S. Finizio, J. Raabe, J. Xia, Y. Zhou, M. Ezawa, X. Liu, J. Chang, H. C.

Koo, Y. Duck Kim, M. Chshiev, A. Fert, H. Yang, X. Yu, and S. Woo, arXiv:1907.01425.

[23] Y. Deng, Y. Yu, Y. Song, J. Zhang, N. Z. Wang, Z. Sun, Y. Yi, Y. Z. Wu, S. Wu, J. Zhu, J. Wang, X. H. Chen, and Y. Zhang, Nature (London) **563**, 94 (2018).

[24] H.-J. Deiseroth, K. Aleksandrov, C. Reiner, L. Kienle, and R. K. Kremer, Eur. J. Inorg. Chem. **2006**, 1561 (2006).

[25] S. Liu, X. Yuan, Y. Zou, Y. Sheng, C. Huang, E. Zhang, J. Ling, Y. Liu, W. Wang, C. Zhang, J. Zou, K. Wang, and F. Xiu, npj 2D Mater. Appl. **1**, 30 (2017).

[26] Z. Fei, B. Huang, P. Malinowski, W. Wang, T. Song, J. Sanchez, W. Yao, D. Xiao, X. Zhu, A. F. May, W. Wu, D. H. Cobden, J.-H. Chu, and X. Xu, Nat. Mater. **17**, 778 (2018).

[27] A. T. Costa, R. B. Muniz, and D. L. Mills, Phys. Rev. B **69**, 064413 (2004).

[28] A. T. Costa, R. B. Muniz, and D. L. Mills, Phys. Rev. B **70**, 054406 (2004).

[29] A. T. Costa, R. B. Muniz, and D. L. Mills, Phys. Rev. B **74**, 214403 (2006).

[30] P. Buczek, A. Ernst, and L. M. Sandratskii, Phys. Rev. B **84**, 174418 (2011).

[31] P. Buczek, A. Ernst, and L. M. Sandratskii, Phys. Rev. Lett. **106**, 157204 (2011).

[32] J. Rajeswari, H. Ibach, C. M. Schneider, A. T. Costa, D. L. R. Santos, and D. L. Mills, Phys. Rev. B **86**, 165436 (2012).

[33] E. Michel, H. Ibach, C. M. Schneider, D. L. R. Santos, and A. T. Costa, Phys. Rev. B **94**, 014420 (2016).

[34] A. T. da Costa, D. Santos, N. M. R. Peres, and J. Fernández-Rossier, 2D Mater. (2020), doi:10.1088/2053-1583/aba88f.

[35] P. Hohenberg and W. Kohn, Phys. Rev. **136**, B864 (1964).

[36] W. Kohn and L. J. Sham, Phys. Rev. **140**, A1133 (1965).

[37] P. Giannozzi, O. Andreussi, T. Brumme, O. Bunau, M. B. Nardelli, M. Calandra, R. Car, C. Cavazzoni, D. Ceresoli, M. Cococcioni, N. Colonna, I. Carnimeo, A. D. Corso, S. de Gironcoli, P. Delugas, R. A. DiStasio, A. Ferretti, A. Floris, G. Fratesi, G. Fugallo *et al.*, J. Phys.: Condens. Matter **29**, 465901 (2017).

[38] J. P. Perdew, K. Burke, and M. Ernzerhof, Phys. Rev. Lett. **77**, 3865 (1996).

[39] G. Kresse and D. Joubert, Phys. Rev. B **59**, 1758 (1999).

[40] L. A. Agapito, S. Curtarolo, and M. B. Nardelli, Phys. Rev. X **5**, 011006 (2015).

[41] M. B. Nardelli, F. T. Cerasoli, M. Costa, S. Curtarolo, R. D. Gennaro, M. Fornari, L. Liyanage, A. R. Supka, and H. Wang, Comput. Mater. Sci. **143**, 462 (2018).

[42] M. Costa, G. R. Schleder, M. Buongiorno Nardelli, C. Lewenkopf, and A. Fazzio, Nano Lett. **19**, 8941 (2019).

[43] M. Montalti, A. Credi, L. Prodi, and M. Teresa Gandolfi, *Handbook of Photochemistry* (CRC Press, Boca Raton, FL, 2006).

[44] M. Costa, M. Buongiorno Nardelli, A. Fazzio, and A. T. Costa, arXiv:1808.00347.

[45] S. Calder, A. I. Kolesnikov, and A. F. May, Phys. Rev. B **99**, 094423 (2019).

[46] H. L. Zhuang, P. R. C. Kent, and R. G. Hennig, Phys. Rev. B **93**, 134407 (2016).

[47] S. Laref, K.-W. Kim, and A. Manchon, [Phys. Rev. B (to be published)], arXiv:2004.01616.

[48] See Supplemental Material at http://link.aps.org/supplemental/10.1103/PhysRevB.102.014450 for technical details of the calculations and more discussion.

[49] H. J. Qin, K. Zakeri, A. Ernst, L. M. Sandratskii, P. Buczek, A. Marmodoro, T.-H. Chuang, Y. Zhang, and J. Kirschner, Nat. Commun. **6**, 6126 (2015).

[50] A. J. Princep, R. A. Ewings, S. Ward, S. Tóth, C. Dubs, D. Prabhakaran, and A. T. Boothroyd, npj Quantum Mater. **2**, 63 (2017).